Phys. Lett. B 860 (2025) 139188

Contents lists available at ScienceDirect

Physics Letters B

journal homepage: www.elsevier.com/locate/physletb

Letter

Internal structure of the $T_{cc}(3875)^+$ from its light-quark mass dependence

Michael Abolnikov [a], Vadim Baru [a,*], Evgeny Epelbaum [a], Arseniy A. Filin [a], Christoph Hanhart [b], Lu Meng [a]

[a] Institut für Theoretische Physik II, Ruhr-Universität Bochum, D-44780 Bochum, Germany
[b] Institute for Advanced Simulation (IAS-4), Forschungszentrum Jülich, D-52425 Jülich, Germany

ARTICLE INFO

Editor: B. Grinstein

ABSTRACT

We employ a chiral effective field theory-based approach to connect DD^* scattering observables at the physical and variable pion masses accessible in lattice QCD simulations. We incorporate all relevant scales associated with three-body $DD\pi$ dynamics and the left-hand cut induced by the one-pion exchange for pion masses higher than the physical one, as required by analyticity and unitarity. By adjusting the contact interactions to match experimental data at the physical pion mass and lattice finite-volume energy levels at $m_\pi = 280$ MeV, we predict the trajectory of the T_{cc} pole as a function of the pion mass, finding it consistent with the hadronic-molecule scenario. In particular, we find that the explicit treatment of the one-pion exchange has a pronounced effect on the pole trajectory for $m_\pi \gtrsim 230$ MeV by pushing it into the complex energy plane.

1. Introduction

The spectroscopy of mesons and baryons containing hidden and open heavy flavor quarks has made tremendous progress in recent years. Experimental observations have provided evidence for numerous multiquark exotic states, including tetraquarks for mesons and pentaquarks for baryons, with many of them being found in close proximity to certain hadron-hadron thresholds, as summarized in recent reviews [1–8]. However, the structure of these exotic hadrons, determined by the internal clustering of quarks, is largely unknown and remains the subject of extensive research. Prominent theoretical scenarios for these structures include hadronic molecules, compact multiquark states and atom-like hadronic configurations called hadroquarkonia, where a compact heavy quarkonium serves as a core. The size of a molecule made out of two hadrons is controlled by the inverse binding momentum $\gamma = \sqrt{2\mu E_B}$, where E_B denotes the binding energy and μ the reduced mass of the hadrons. Thus, for very small binding energies, hadronic molecules acquire a very large size: The state of interest for this paper has $E_B \approx 300$ keV, yielding a spatial extension of the order of $1/\gamma \approx 8$ fm. Conversely, compact states are characterized by a size of the order of $1/\Lambda_{\rm QCD} \simeq 1$ fm, where $\Lambda_{\rm QCD}$ represents the typical scale of the strong interactions.

In 2021, the LHCb experiment discovered the first exotic doubly-charmed narrow resonance, denoted as $T_{cc}(3875)^+$, whose minimal quark composition is $cc\bar{u}\bar{d}$ [9,10]. This discovery revealed a state with a mass just a few hundred keV below the $D^{*+}D^0$ threshold, with a width primarily dictated by its strong decay mode to $DD\pi$. Since approximately 90% of the $D^0D^0\pi^0$ events contain a genuine D^* meson [10], it is natural to expect (see the discussions in Refs. [11–13]) that the width of the $T_{cc}(3875)^+$ should be smaller than that of the D^*, which is only (83.4 ± 1.8) keV [14]. The properties of this state have been investigated employing low-energy effective field theories (EFT) [15–20] and phenomenological models, see, e.g., [7] and references therein. In particular, the pole position of the $T_{cc}(3875)^+$ and the DD^* scattering parameters were extracted in Ref. [17] using the leading order chiral EFT approximation by performing a coupled-channel analysis of the experimental line shape in the $D^0D^0\pi^+$ final state. In that work, a special attention was paid to the inclusion of three-body cuts, which were found to be crucial for the accurate determination of the T_{cc} pole position in the complex energy plane. We emphasize that for the T_{cc}, including the one-pion exchange (OPE) to all orders with a proper treatment of its cuts is needed for theoretical consistency. To illustrate this, we note that the D^* self-energy induces an imaginary part to the D^*D propagator, which corresponds to the $DD\pi$ intermediate state going on shell. This on-shell intermediate state contains a pair of identical mesons (DD) in isospin 1, which has to be in an even partial wave to comply with Bose symmetry. Proper symmetrization of the DD state, that ensures this, generates a one-pion exchange. Moreover, since the D^* self-energy is resummed in the D^*D propagator, consistency with Bose symmetry requires resum-

* Corresponding author.
E-mail address: vadimb@tp2.rub.de (V. Baru).

https://doi.org/10.1016/j.physletb.2024.139188
Received 26 July 2024; Received in revised form 6 December 2024; Accepted 7 December 2024

Available online 11 December 2024

ming the OPE as well. For a similar discussion on the Pauli principle in the context of two identical nucleons in the three-body intermediate state, see Refs. [21–23].

More recently, DD^* scattering has also been investigated in lattice QCD employing the Lüscher method [24–27] and the HAL QCD approach [28]. In particular, the analysis performed in Ref. [24] by utilizing the effective range approximation (ERE) suggests that the T_{cc} state is consistent with a virtual state at the pion mass $m_\pi = 280$ MeV. However, two significant concerns have been raised in the literature regarding this conclusion. First, it was emphasized in Ref. [29] that the ERE is only valid for parameterizing the near-threshold energy behavior of the inverse scattering amplitude if there are no nearby left-hand cuts (lhc) generated by long-range interactions. The presence of the OPE in the DD^* scattering potential introduces a left-hand branch point at the center-of-mass momentum $|p^{1\pi}_{\rm lhc}| = 126$ MeV for the given pion mass, thereby significantly restricting the applicability of the effective range expansion. The second issue concerns the Lüscher method that is widely used for extracting infinite-volume scattering amplitudes from finite-volume energy levels calculated on the lattice [30–33], see also [34,35] for generalizations to moving two-body systems and [36–40] for recent reviews. Recent studies have argued that this method faces difficulties in situations involving nearby left-hand cuts [41–44]. Consequently, several extensions of this method or alternative approaches have been proposed to address this issue [41,44–46]. In particular, in Ref. [44], a solution of the lhc problem was proposed based on the chiral EFT approach. Due to the explicit account for the longest-range interaction from the OPE in this approach, finite-volume energy levels can be directly calculated as solutions of the eigenvalue problem both below and above the left-hand cut. The distinctive feature of Ref. [44] is that it not only provided an alternative to the Lüscher method, which is valid in the presence of the lhc, but also allowed, for the first time, to take into account the left-hand cut effects in the analysis of the actual lattice data. Using the lattice energy levels from Ref. [24] and taking into account the lhc effects, Ref. [44] found the T_{cc} to have a 85% probability of being a resonance state (based on the scattering amplitude calculated at the 1σ confidence level), while the remaining 15% probability corresponds to a scenario with two virtual poles [44]. The single virtual pole extracted in Ref. [24] is incompatible with the presence of the left-hand cut, as was already shown in Ref. [29].

In this work, we employ the same chiral EFT-based approach to scrutinize the analytic structure of the scattering amplitude as a function of the pion mass. Given the intricate interplay between the right-hand (three-body) and left-hand cuts, which depend sensitively upon the pion mass, we incorporate all energy and/or momentum scales relevant for this complicated dynamics to predict the pole trajectory of the T_{cc} state for pion masses between the physical value $m_\pi^{\rm ph}$ and $3m_\pi^{\rm ph}$. This information can serve as a benchmark for future lattice QCD calculations and is important for obtaining additional insights into the structure of T_{cc} state [47]. Our analysis also yields predictions for the DD^* phase shifts at any value of m_π within the considered range, in spite of the fact that the ERE has a very limited range of validity. The lhc also necessitates an improvement of the Weinberg approach to properly describe the compositeness of a hadronic state. Besides the fact that the zeros in the T-matrix emerging from the interplay of the repulsive OPE potential and attractive short-range physics may invalidate the original Weinberg formalism, as discussed in Refs. [48–50], already the small scale introduced into the system by the nearby lhc calls for a refined formulation of the compositeness criterion.

2. Framework

In this work, we use both experimental data [9,10] and lattice energy levels [24] to determine the a priori unknown low-energy constants in chiral EFT. With these fixed, we predict the DD^* scattering amplitude at various pion masses. Before discussing the explicit procedure, several remarks are in order:

- We focus on observables near the DD^* threshold, so we do not consider potential coupled-channel effects involving D^*D^*. In a very recent lattice investigation of coupled-channel $DD^* - D^*D^*$ scattering at $m_\pi = 391$ MeV, a sizeable coupled-channel effect was reported [26] within the Lüscher formalism using, however, amplitude parameterizations that ignore the left-hand cuts. We briefly comment on these results below. However, since no information about the coupled-channel dynamics is available from Ref. [24], which is used as input for our study, these effects are ignored.
- Our calculations are performed in the isospin limit using the averaged masses $M_{D^{(*)}} = (M_{D^{(*)0}} + M_{D^{(*)c}})/2$ for the $D^{(*)}$-mesons. Additionally, since electromagnetic effects are not yet resolved on the lattice, we ignore the radiative decay width of the D^*, considering only its strong pionic decay.
- The main goal of this study is to analyze the pion mass dependence of DD^* scattering observables in the continuum limit. The lattice energy levels used here as input are obtained at a single lattice spacing of $a \approx 0.086$ fm. Previous investigations, such as Ref. [51], found the dependence of finite volume energy levels on the lattice spacing in the doubly heavy sector to be moderate for the $ud\bar{c}\bar{c}$ case. Based on these findings, we neglect the lattice spacing dependence in our analysis.

The effective potential V for DD^* scattering is constructed in chiral EFT up to $\mathcal{O}(Q^2)$, where $Q = p/\Lambda_b$ with $p \sim m_\pi$ being a characteristic soft momentum scale and Λ_b referring to the breakdown scale of the chiral expansion, and is given by

$$V = V^{(0)}_{\rm OPE} + V^{(0)}_{\rm cont} + V^{(2)}_{\rm cont} + \dots \,. \tag{1}$$

Here, we assume that the two-pion exchange contributions are largely saturated by the contact terms, see also Refs. [52,53] for related studies in the context of the $X(3872)$.

In analogy to the NN system [54,55], it was shown in Ref. [56] that the OPE potential in heavy-meson systems is well defined, in the EFT sense, only in combination with contact operators. These contact terms account for our ignorance of short-range dynamics and have the form of a polynomial function in the pion mass and momenta. The isoscalar contact potentials contributing to the relevant ${}^3S_1$[1] partial wave near the DD^* threshold can be parametrized as

$$\begin{aligned} V_{\rm cont}(p,p') &= \left[c_0(\xi) + c_2(\xi)(p^2 + p'^2)\right](\epsilon\cdot\epsilon'^*)\,, \\ c_0(\xi) &= C_0 + D_2(\xi^2 - 1) + \mathcal{O}(\xi^4, p^4)\,, \\ c_2(\xi) &= C_2 + \mathcal{O}(\xi^2)\,, \end{aligned} \tag{2}$$

where $\xi = m_\pi/m_\pi^{\rm ph}$ while $\boldsymbol{p}$ ($\boldsymbol{p}'$) and $\boldsymbol{\epsilon}$ ($\boldsymbol{\epsilon}'$) denote the center-of-mass momentum and polarization of the initial (final) D^* meson, respectively. The values of the low-energy constants (LECs) in Eq. (2) are determined from empirical data at the physical pion mass ($\xi = 1$) as well as from the lattice energy levels at certain ξ-values away from the physical point, as discussed in Sec. 3. In this work, for this purpose, we use the lattice QCD data at $m_\pi = 280$ MeV, which corresponds to $\xi \approx 2$. The effect of higher-order contact terms at $\mathcal{O}(Q^4)$ is estimated in Sec. 4.

In the framework of time-ordered-perturbation theory (TOPT), the isoscalar OPE potential is given by

$$V_{\rm OPE}(E,\boldsymbol{p},\boldsymbol{p}') = -\frac{g^2}{8f_\pi^2}\frac{(\boldsymbol{q}\cdot\boldsymbol{\epsilon})(\boldsymbol{q}\cdot\boldsymbol{\epsilon}'^*)}{2\omega_\pi(\boldsymbol{q}^2)}\,D^\pi(E,\boldsymbol{p},\boldsymbol{p}'), \tag{3}$$

where f_π is the pion decay constant and g is the coupling constant of pions with heavy mesons. Furthermore,

[1] Here and in what follows, we use the spectroscopic notation ${}^{2S+1}L_J$ to indicate a DD^* partial wave with total spin S, angular momentum L and total angular momentum equal to J.

$$D^{\pi}(E,\boldsymbol{p},\boldsymbol{p}') = D_1(E,\boldsymbol{p},\boldsymbol{p}') + D_2(E,\boldsymbol{p},\boldsymbol{p}'), \tag{4}$$

and the two TOPT propagators read

$$D_1(E,\boldsymbol{p},\boldsymbol{p}') = \left(2M_D + \frac{p^2+p'^2}{2M_D} + \omega_\pi(\boldsymbol{q}^2) - E - i\epsilon\right)^{-1},$$

$$D_2(E,\boldsymbol{p},\boldsymbol{p}') = \left(2M_{D^*} + \frac{p^2+p'^2}{2M_{D^*}} + \omega_\pi(\boldsymbol{q}^2) - E - i\epsilon\right)^{-1}.$$

Here, E is total energy of the system and $\boldsymbol{q}=\boldsymbol{p}+\boldsymbol{p}'$. We treat the pion relativistically, such that $\omega_\pi(\boldsymbol{q}^2)=\sqrt{m_\pi^2+\boldsymbol{q}^2}$, while the $D^{(*)}$ mesons are nonrelativistic. The resulting potential can be therefore written as

$$V(E,\boldsymbol{p},\boldsymbol{p}') = V_{\rm cont}(p,p') + V_{\rm OPE}(E,\boldsymbol{p},\boldsymbol{p}'). \tag{5}$$

The partial-wave-projected potentials $V_{\alpha\beta}(E,p,p')$ are obtained along the lines of Refs. [57,58] as follows,

$$V_{\alpha\beta}(E,p,p') = \frac{1}{2J+1}\int \frac{d\Omega_p}{4\pi}\frac{d\Omega_{p'}}{4\pi} \times {\rm Tr}\Big[P^\dagger(JLS;\boldsymbol{n})V(E,\boldsymbol{p},\boldsymbol{p}')P(JL'S';\boldsymbol{n}')\Big], \tag{6}$$

where the Greek indices run from 1 to 2 accounting for the ${}^3S_1$ and ${}^3D_1$ partial waves, respectively, with $L(L')=S$ or D; $\boldsymbol{n}=\boldsymbol{p}/p$ ($\boldsymbol{n}'=\boldsymbol{p}'/p'$), and a complete set of relevant properly normalized projection operators $P(JLS;\boldsymbol{n})$ is given in the Appendix of Ref. [58].

The scattering amplitude is calculated as a solution of the Lippmann-Schwinger equation

$$T_{\alpha\beta}(E,p,p') = V_{\alpha\beta}(E,p,p') + \int_0^\Lambda \frac{{\rm d}q\, q^2}{2\pi^2} V_{\alpha\gamma}(E,p,q)G(E,q)T_{\gamma\beta}(E,q,p'). \tag{7}$$

In order to render the integral in (7) well defined, we use a sharp cutoff regularization. Specifically, the main results were obtained using $\Lambda = 700$ MeV, but for the purpose of testing the cutoff dependence we also use $\Lambda = 500$ MeV. The DD^* propagator is expressed as

$$G(E,q) = \left[M_{D^*} + M_D + \frac{q^2}{2\mu} - E - \frac{i}{2}\Gamma(E,q)\right]^{-1}, \tag{8}$$

where $\mu = M_D M_{D^*}/(M_D+M_{D^*})$ is the reduced mass,

$$\Gamma(E,q) = \frac{g^2 M_D}{8\pi f_\pi^2 M_{D^*}}\Big[\Sigma(s) - \Sigma_0(s)\theta(M_D+m_\pi-M_{D^*})\Big]$$

is the dynamical width of the D^* with

$$\Sigma(s) = \left[\frac{\sqrt{\lambda(s,M_D^2,m_\pi^2)}}{2\sqrt{s}}\right]^3, \tag{9}$$

and $\lambda(a,b,c) = a^2+b^2+c^2-2ab-2bc-2ca$ is the Källén triangle function, and $s=[E-M_D-q^2/(2\mu)]^2$. Here

$$\Sigma_0(s) = \Sigma(M_{D^*}^2) + 2M_{D^*}\left(E - M_{D^*} - M_D - \frac{q^2}{2\mu}\right)\Sigma'(M_{D^*}^2),$$

where the first and second terms renormalize the D^* mass and wave function, respectively, if $M_{D^*} < M_D + m_\pi$. The dependence of the D- and D^*-meson masses on m_π was explored in Ref. [59] using unitarized SU(3) chiral perturbation theory. The tree-level expressions for M_D and M_{D^*}, derived from the expansion around the physical masses with the charm quark mass kept at its physical value, are as follows,

$$M_D(\xi) = M_D^{\rm ph}\left[1 + h_1\left(\frac{m_\pi^{\rm ph}}{M_D^{\rm ph}}\right)^2(\xi^2-1)\right], \tag{10}$$

$$M_{D^*}(\xi) = M_{D^*}^{\rm ph}\left[1 + h_1\left(\frac{m_\pi^{\rm ph}}{M_{D^*}^{\rm ph}}\right)^2(\xi^2-1)\right], \tag{11}$$

where $h_1 \approx 0.42$. The pion mass dependence of the pion decay constant f_π and the πDD^* coupling constant g is considered along the lines of Refs. [29,60] — see Sec. 3 of the Supplemental Material in Ref. [29]. Note also that the extraction of the coupling constant g was recently updated in Ref. [29] by making two-dimensional fits of lattice data [60] with simultaneously varied m_π and the lattice spacing. We have verified that employing the updated coupling has a small impact, which lies well within the theoretical uncertainty of the results discussed in Sec. 4. We therefore do not dwell on this any further.

3. Pole position as a function of the pion mass

3.1. LO *results*

Before discussing the next-to-leading order (NLO) results in the following section, it is worth noting that all pole trajectories for this problem exhibit several common features, which we can illustrate using the leading-order (LO) results. In chiral EFT at LO, there is only one contact term, C_0 (see Eq. (2)) which is adjusted to reproduce the real part of the T_{cc} pole position, ${\rm Re}\,E_{\rm pole} = -356$ keV, extracted in Ref. [17] (see "pionful fit III" in Table II) from a chiral EFT-based analysis of the experimental data. The imaginary part of the T_{cc} pole at the physical pion mass is governed by its three-body decay to $DD\pi$ and, therefore, comes out as a prediction since the $D^*D\pi$ coupling is known. Then, the T_{cc} pole trajectory for pion masses other than the physical one is predicted based on the interplay of several scales, primarily associated with the OPE, as discussed below.

The analytic structure of the scattering amplitude in the complex momentum plane (k-plane) is continuously changing with varying pion mass. At the nominal D^*D threshold, the OPE has both a real and an imaginary part as long as the three-body $DD\pi$ threshold is below the DD^* threshold. This is fulfilled, in particular, for the physical pion mass ($\xi = 1$). Defining the on-shell momentum relative to the two-body threshold by k, with $E = M_D + M_{D^*} + k^2/(2\mu)$, and introducing $\Delta M = M_{D^*} - M_D$, the three-body branch point can be found by requiring $E_{\rm rhc_3} = M_D + M_{D^*} + k_{\rm rhc_3}^2/(2\mu) = 2M_D + m_\pi$. This leads to

$$k_{\rm rhc_3}^2 = 2\mu(m_\pi - \Delta M). \tag{12}$$

This relation can also be derived by setting $p=p'=0$ in the propagator D_1 in Eq. (4), resulting in $k_{\rm rhc_3}^2 < 0$ and $|k_{\rm rhc_3}| \approx 88$ MeV at the physical pion mass. Even when p and p' are different from zero, the cut can still occur at the given pion mass, if the denominator in D_1 vanishes. However, in these cases, it will emerge at $k^2 > k_{\rm rhc_3}^2$.

When both p and p' are on shell ($p=p'=k$) and $m_\pi > \Delta M$, the OPE and, consequently, the on-shell DD^* partial wave amplitudes, exhibit the left-hand cut at imaginary values of the momenta. The lhc branch point closest to the threshold is given by [29]

$$(k_{\rm lhc}^{1\pi})^2 \approx \frac{1}{4}[(\Delta M)^2 - m_\pi^2]. \tag{13}$$

This can be derived from D_1 using that $\mu \approx m_D/2$, leading to the conclusion that $\omega_\pi(4k^2) = \Delta M$ for forward DD^* scattering ($\cos(\boldsymbol{p}\cdot\boldsymbol{p}') = 1$).

The partial-wave projected OPE potential with both initial and final D^*D pair on-shell can exhibit either a lhc or a three-body cut, depending on the pion mass, as illustrated in Fig. 1. When the pion mass increases from its physical value, the three-body phase space closes rapidly as the decay of $D^* \to D\pi$ becomes kinematically forbidden at $\xi = \xi_0 \approx 1.03$. Consequently, the three-body cut in the on-shell partial-wave projected OPE potential turns into the lhc.

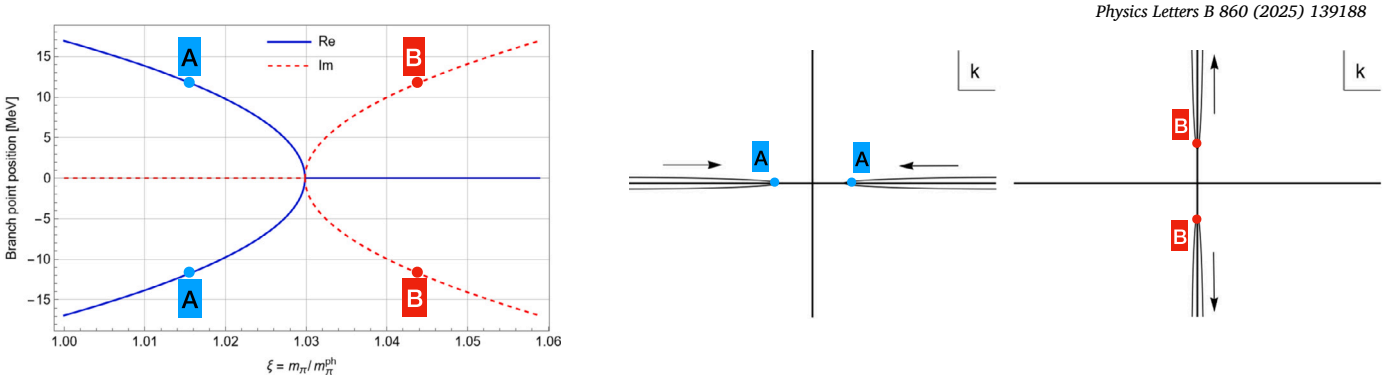

Fig. 1. Branch cuts in the on-shell partial-wave projected OPE potential versus the pion mass. Left panel: Re (blue solid lines) and Im (red dashed lines) parts of the branch point momentum. Real momenta correspond to a three-body cut, imaginary ones to a lhc. At $\xi = \xi_0 \approx 1.03$, the right-hand cut changes into a left-hand cut. Middle and right panel: Schematic behavior of the branch cuts in the complex k plane when the pion mass is increased. The direction of change is indicated by arrows. The blue points A indicate the branch points of the right-hand cut at some value of $\xi \in [1, 1.03]$. The red points B indicate the branch points of the left-hand cut at some value of $\xi > 1.03$.

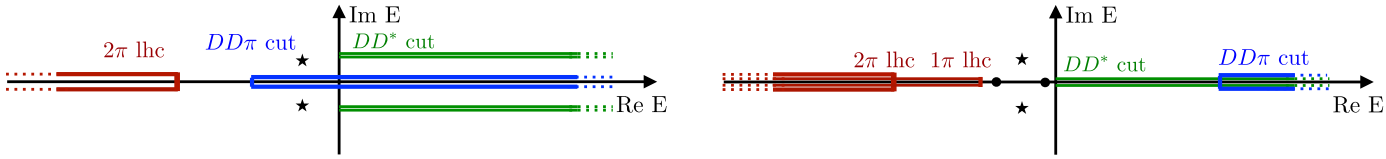

Fig. 2. Sketch of the locations of various branch cuts and poles in the complex energy plane for the physical pion mass (left panel) and $m_\pi = 280$ MeV (right panel). The left-hand cut, the two-body D^*D cut, and the three-body $DD\pi$ cut are shown in red, green, and blue, respectively. The black symbols show typical locations for the T_{cc}^+ poles which show up either as a pair of virtual states (dots) or a resonance (stars) in case for the larger pion mass or as quasi-bound state at the physical pion mass. For the two scenarios the poles are located on the second and first Riemann sheet with respect to the DD^* cut, respectively.

An alternative view on the singularity structure of the problem can be gained by examining the trajectories of the branch points in the complex energy plane of the T-matrix, see Eq. (7) and Fig. 2 for illustration. Starting at the physical pion mass with $\xi = 1$ and $m_\pi < \Delta M$, there are three branch points in the amplitude near the DD^* threshold (see left panel): the lowest in energy is the three-body cut starting from the πDD threshold, followed by a pair of branch points in the second sheet of the complex plane in the propagator G, related to the on-shell two-body D^*D intermediate state. Here, the πDD cut generates the imaginary parts of the D^*D branch points, related to each other via the Schwarz reflection principle. As we increase the pion mass or, equivalently ξ, the three branch points approach each other. At $\xi = \xi_0 \approx 1.03$ the decay of $D^* \to D\pi$ becomes kinematically forbidden and all three branch points coincide. If we increase ξ further, the number of branch points stays the same, but their character changes (see right panel): the left-hand cut from the OPE appears below the D^*D threshold followed in energy by the D^*D branch point, which is now located on the real axis. Even higher up is the $DD\pi$ three-body cut. We emphasize that for all pion masses, besides the special case when $m_\pi = \Delta M$, the branch point of the three-body cut, as per Eq. (12), can only be reached if the incoming and the outgoing D^*D state in the OPE potential is off shell (as discussed above, the three-body cut can still occur in the on-shell potential for $m_\pi < \Delta M$ if the denominator in D_1 vanishes, but only at $k^2 > k^2_{\text{rhc}_3}$, and for $m_\pi = \Delta M$ the branch points of the on-shell and off-shell potentials coincide at $k^2 = 0$). While in the off-shell amplitude this condition comes naturally from the off-shell potential $V_{\alpha\beta}(E, p, p')$ itself, the off-shell potential also enters the on-shell amplitude through iterations.

Additionally, the lhcs from multi-pion exchanges are also present in the amplitude, but are much more distant from the threshold and therefore expected to have negligible impact on the process under consideration.

We now investigate the trajectory of the T_{cc}^+ pole as ξ is varied, which is largely influenced by the non-trivial motion of the branch points described in the previous paragraph. The T_{cc}^+ pole at the physical pion mass can be interpreted as a quasi-bound state – a would be bound state of DD^* if there were no three-body decay to $DD\pi$. When the pion mass increases, the T_{cc}^+ width decreases accordingly and the corresponding pole in the complex momentum plane (k-plane) approaches the imaginary axis, finally turning into a bound state. This is illustrated in Fig. 3 – see the zoomed plot in the left panel. Please note, however, that the imaginary part of the quasi-bound state energy is so small that it is indistinguishable from zero in the right panel of Fig. 3. The proper bound state occurs when the T_{cc}^+ pole, located below the DD^* threshold, coincides with the three-body threshold. This takes place at $\xi = \xi' \approx 1.027$, which is just a bit smaller than ξ_0. Therefore, there is a very narrow range of $\xi_0 > \xi > \xi'$, where the three-body threshold is still below the two-body threshold, but the T_{cc}^+ is already stable. By further departing from the physical point in terms of ξ, the bound state on the physical Riemann sheet (RS-I) turns into a virtual state on RS-II. The particular value of ξ when this happens depends on the dynamics, namely on whether the LO or NLO potential is employed: at LO of the chiral EFT expansion, the transition emerges at $\xi \approx 1.3$. A common feature of all settings is the appearance of the second (lower-lying) virtual pole, the dynamics of which is interrelated with the location of the lhc from the OPE. The general pattern is illustrated in Fig. 3 and is as follows: At some ξ, the second virtual pole occurs from under the lhc branch cut and goes along with the branch point until the first (upper) pole comes close. Then, both poles collide and the state becomes a resonance. The OPE plays a significant role, not only by providing a repulsion, which would be absent in a pure contact formulation, but also affecting the analytic properties of the DD^* scattering amplitude in a very nontrivial way. The right panel of Fig. 3 shows the behavior of the pole in the energy plane that corresponds to the k-plane pole trajectory in the left panel. The cusps and the point where $E_{\text{pole}} = 0$ indicate a change in the character of the pole, which transitions from a quasi-bound to bound, virtual and finally to a resonance state as ξ increases. The point where $E_{\text{pole}} = 0$ corresponds to the transition from RS-I to RS-II. Qualitatively, the pole trajectories described here are similar to those discussed, e.g., in Refs. [47,61–64], though modified by the effects of dynamical pions. These pionic effects induce the only hadronic contribution to the

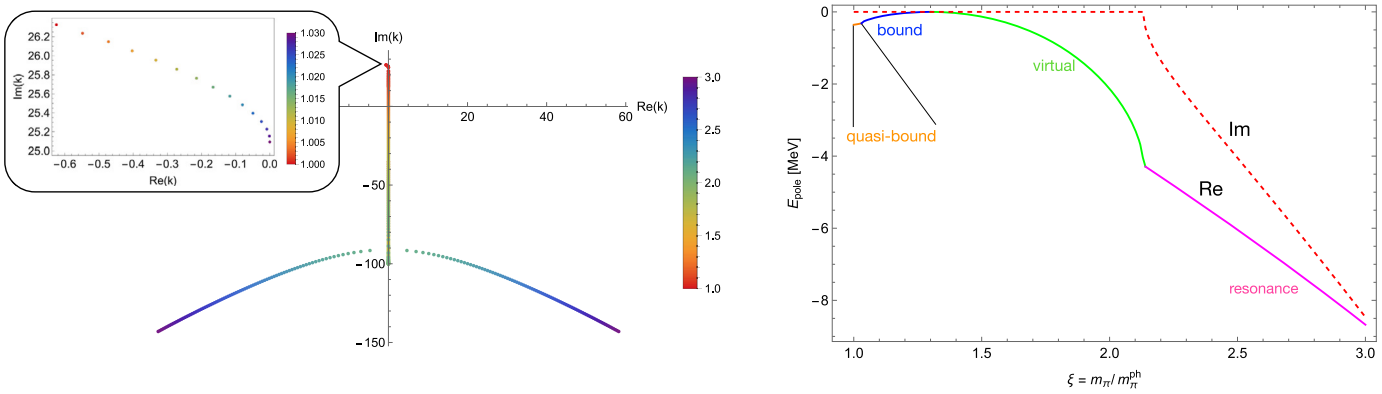

Fig. 3. Left panel: Pion mass dependence of the T_{cc} pole in the complex k-plane predicted at LO in chiral EFT. The value of ξ is indicated by color. The second, more distant virtual state is also shown, along with its collision point with the T_{cc} pole, after which the resonance poles emerge. Right panel: LO trajectory of the T_{cc} pole in the complex energy plane as a function of ξ, corresponding to the left panel. Re $E_{\rm pole}$ and Im $E_{\rm pole}$ are shown by solid and dashed lines, respectively. The second, more distant state is not shown; only the energy of the pole with $\mathrm{Re}(k) > 0$ is shown after the resonance appears.

imaginary part of the T_{cc} pole at the physical point and influence the ξ dependence of the T_{cc} pole as well as the second more distant virtual pole.

3.2. NLO *results*

While the results at LO capture the behavior of the pole trajectory qualitatively, in this section, we discuss how the results change when the higher-order contact interactions in Eq. (2), C_2 and D_2, are incorporated. First, we note that the experimental data [9,10] do not allow us to fix the momentum-dependent $\mathcal{O}(Q^2)$ LEC C_2 — or stated otherwise, at the physical point there is a strong correlation between the values of C_2 and C_0. Accordingly, the EFT-based analysis of Ref. [29] resulted in an excellent description of the experimental line shapes using $C_2 = 0$. On the other hand, this momentum-dependent short-range interaction was found to be important in Refs. [29,44] for understanding the results of Ref. [24] at $m_\pi = 280$ MeV ($\xi \approx 2$). To extract the unknown parameters of the short-range interactions at $\mathcal{O}(Q^2)$ — specifically, C_2 and D_2 in Eq. (2) — we use the phase shifts extracted in [44] from the lattice energy levels at $\xi \approx 2$ [24]. It is important to emphasize that the LECs extracted in Ref. [44] cannot be used directly in the current analysis, since Ref. [44] approximates the full πDD Green function, as per Eq. (4), with the static pion propagator. While this approximation is justified for analyzing lattice data at $m_\pi = 280$ MeV, the three-body cut emerging from the πDD Green function is crucial for maintaining the correct analytic structure of the DD^* scattering amplitude and thus for providing chiral extrapolations from the lattice data to the physical point. Thus, we adjust the contact terms to the phase shifts with the main criterion that the resulting central curve and its uncertainty band should resemble those from Ref. [44]. The results of our best fit, including the 1σ uncertainty band, are shown in Fig. 4, along with the original phase shifts from Ref. [44], and are in good agreement. However, we note that we do not account for possible correlations between the input data points. This leads to a more conservative estimate of the propagated uncertainty. To propagate the uncertainties from the original dataset into our calculations, we use the bootstrap procedure — see, e.g., Ref. [65] for details. Specifically, we employ the orange band in Fig. 4 from Ref. [44] to randomly generate 1000 datasets, assuming a Gaussian distribution. Each of these simulated datasets is individually used to determine the best-fit parameters C_2 and D_2. The resulting distribution of $\{C_2, D_2\}$ from these fits is then propagated to estimate the uncertainty of the results for the DD^* scattering amplitude and the T_{cc} pole position. This uncertainty is associated with the statistical uncertainty of the finite-volume energy levels from Ref. [24].

In Fig. 5, we show the results for the pole position at NLO in chiral EFT. As a general pattern, one finds that the subleading short-range

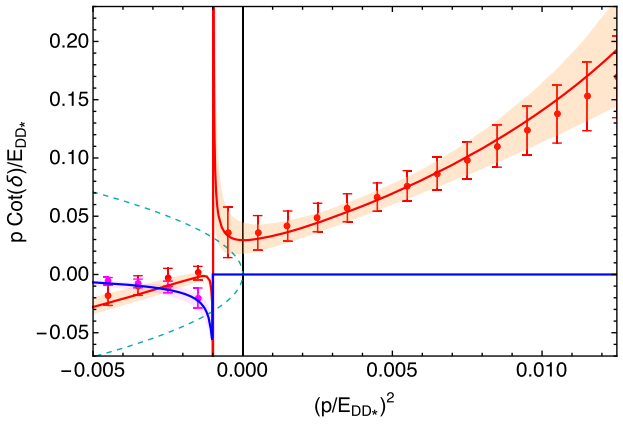

Fig. 4. Fit to the DD^* scattering phase shifts, which were extracted previously in Ref. [44] from FV energy levels, including the lhc from the OPE. Red and pink dots denote the real and imaginary parts of $p\cot\delta$ in the ${}^3S_1$ partial wave from Ref. [44]. Red and blue lines are the results of the best fit for the real and imaginary parts obtained in this work; orange and pink bands represent the 1σ uncertainty. Cyan dashed line corresponds to $ip = \pm|p|$ from unitarity. $E_{DD*} = M_D + M_{D*}$.

interaction provides additional repulsion, causing both the transitions from bound to virtual state (when Re $E_{\rm pole}$ crosses 0) and from virtual state to a resonance to occur at lower values of ξ compared to LO. The D-wave contribution from the OPE is found to play a minor role in the pole trajectory, as seen by comparing the solid (pure S wave) and dashed (with D wave included) red lines in Fig. 5. Given the smallness of this effect, we neglect the D wave components when performing uncertainty quantification. This especially helps to simplify the bootstrap procedure used to estimate statistical uncertainty of the results.

In Fig. 6, we compare our NLO results with the pole trajectory obtained from a pure contact theory using only the contact potential from Eq. (2) (see the dashed-dotted line). The LECs for the contact potential were obtained by reproducing the physical value of the T_{cc} pole position and the phase shifts of Ref. [24], which were extracted from the finite-volume spectra using the Lüscher method and analyzed employing the ERE. We note that a recent lattice investigation of coupled $DD^* - D^*D^*$ scattering at $m_\pi = 391$ MeV ($\xi \approx 2.85$) [26], also using the Lüscher method and ignoring the lhc, predicts a virtual state 62 ± 34 MeV below the DD^* threshold, fully consistent with the about 75 MeV virtual state predicted by our dot-dashed curve. In addition, the virtual state pole obtained by extrapolating the ERE from Ref. [25] to the below-threshold region (see the green point) is also in line with the prediction from our contact EFT. On the other hand, it is evident that the

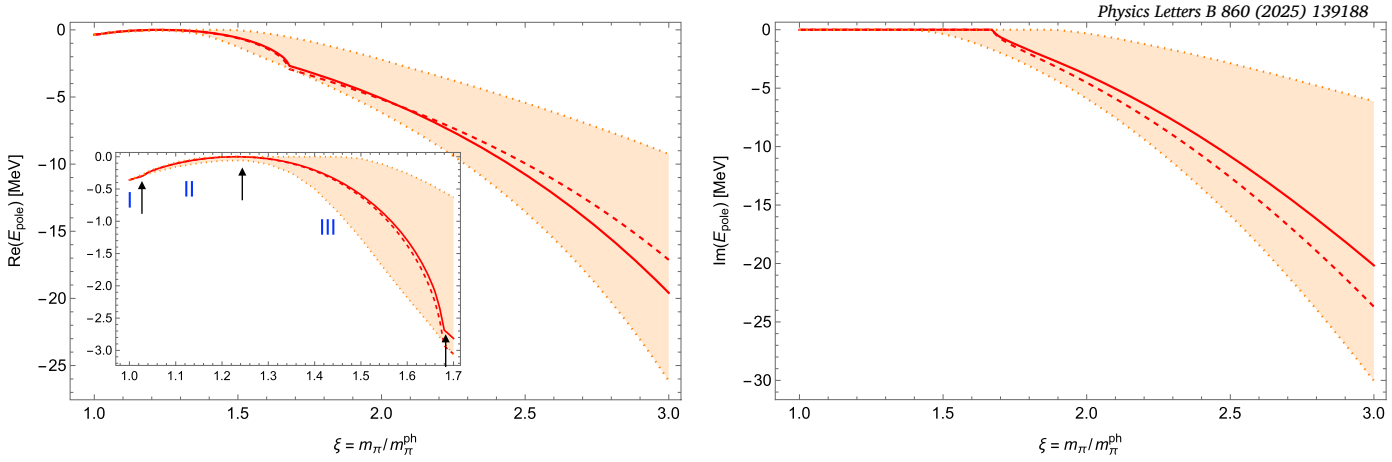

Fig. 5. The real (left panel) and imaginary (right panel) parts of the T_{cc} pole position at NLO in chiral EFT as a function of the pion mass. The solid red line corresponds to the best fit at NLO with the S-wave OPE potential, while the orange band stands for the 1σ error band estimated using bootstrap. The dashed red line corresponds to the best fit at NLO with the full OPE potential, including D waves. The inlay highlights the behavior of the pole at lower pion masses, where the transition from quasi-bound (region I) to bound (region II), and then to virtual state occurs (region III), as indicated by the arrows. After $\xi \approx 1.68$ the T_{cc} becomes a resonance state and the Im part of the pole occurs in the right panel.

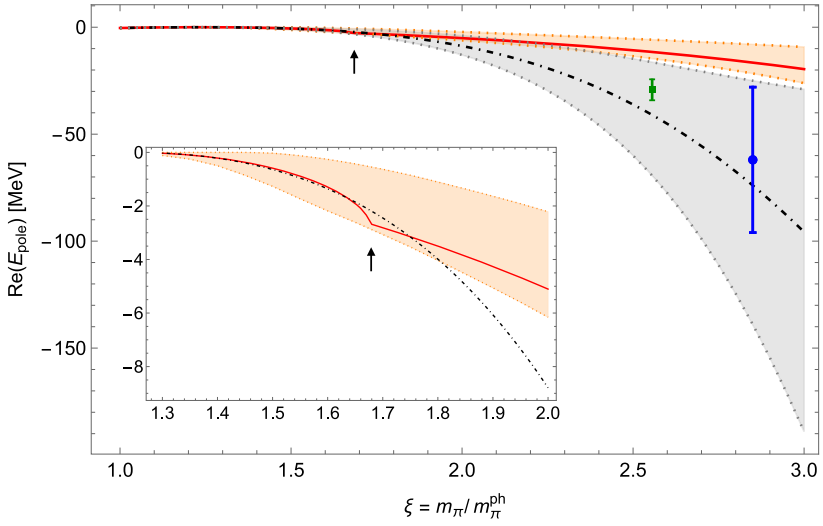

Fig. 6. Comparison of the T_{cc} pole trajectory at NLO in chiral EFT with that in a pionless (contact) theory (dot-dashed line). Notation is the same as in Fig. 5. Only the real part is shown, as the pole in the contact theory is always real; gray band indicates the statistical uncertainty of the contact EFT calculation propagated from fits to the lattice energy levels based on the ERE [24]. The arrow indicates the pion mass ($\xi \approx 1.68$), after which the pole in the pionful theory becomes a resonance state while the pole in the pionless theory remains a virtual state. The blue data point corresponds to a virtual state extracted by the Hadron Spectrum Collaboration at $m_\pi = 391$ MeV [26], while the green square corresponds to a virtual state at $m_\pi \approx 348.5$ MeV, extracted using the ERE parameters from Ref. [25].

additional repulsion from the longest-range OPE potential, not included in Refs. [25,26], significantly impacts the results. Unlike the contact trajectory, which remains a virtual state with growing pion mass, our NLO pole position transforms from a virtual state to a resonance at pion masses corresponding to $\xi \approx 1.7$.

The behavior of the T_{cc} pole trajectory with respect to the pion mass predicted in Figs. 3 and 5 is consistent with a molecular nature of the T_{cc} state. Indeed, the smooth transition of the pole trajectory from a bound state to a virtual state as the light-quark mass changes is a distinguishing feature of a molecular structure [47].

4. Theoretical uncertainty and cross checks

4.1. Chiral truncation error

In the previous section, we presented the results for the T_{cc} pole trajectory and estimated errors by propagating the statistical uncertainty of the lattice data. In this section, we provide an estimate of the theoretical uncertainty which comes from the truncation of the chiral expansion and the cutoff dependence.

The uncertainty associated with the truncation of the chiral expansion can be estimated by introducing the higher-order $\mathcal{O}(Q^4)$ terms, not explicitly included in the calculations so far, and evaluating their impact on the results. The $\mathcal{O}(Q^4)$ terms used for the uncertainty quantification are

$$V_{\rm cont}^{(4)} = D_4(\xi^2 - 1)(p^2 + p'^2) + \tilde{D}_4(\xi^4 - 1), \tag{14}$$

while the effect of the m_π-independent $\mathcal{O}(p^4)$ contact term is neglected, as this is consistent with available experimental information at $m_\pi = m_\pi^{ph}$ and lattice data at $m_\pi = 280$ MeV. Here, D_4 and $\tilde{D}_4$ can be expressed as

$$D_4 = \frac{\alpha_4}{F_\pi^2}\left(\frac{m_\pi^{ph}}{\Lambda_\chi^2}\right)^2, \qquad \tilde{D}_4 = \frac{\tilde{\alpha}_4}{F_\pi^2}\left(\frac{m_\pi^{ph}}{\Lambda_\chi}\right)^4, \tag{15}$$

with $\Lambda_\chi \simeq 1$ GeV being the chiral symmetry breaking scale. Here, α_4 and $\tilde{\alpha}_4$ are dimensionless prefactors expected to be of the order of 1

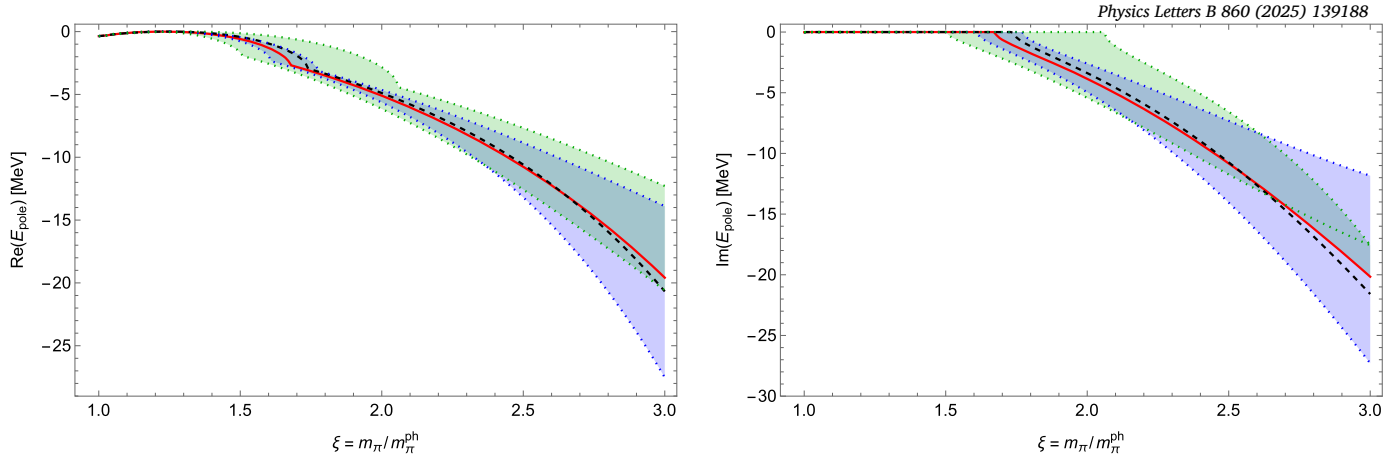

Fig. 7. Theoretical uncertainty for the T_{cc} pole position. The bands represent the truncation uncertainty of the chiral expansion for the T_{cc} pole position at $\Lambda = 700$ MeV when the $\mathcal{O}(Q^4)$ terms in Eq. (14) are included. The green band corresponds to the variation of the dimensionless constant α_4 in the range $[-1, 1]$, while the blue band corresponds to the variation of the dimensionless constant $\tilde{\alpha}_4$ in the same range. Red solid and black dashed lines represent the best fits for $\Lambda = 700$ MeV and $\Lambda = 500$ MeV, respectively.

based on naturalness, as discussed analogously in the NN case [66]. Indeed, applying the same logic to the terms C_2 and D_2 in Eq. (2), we can rewrite them in the following form,

$$C_0 = \frac{\alpha_0}{F_\pi^2}, \quad C_2 = \frac{\alpha_2}{F_\pi^2}\frac{1}{\Lambda_\chi^2}, \quad D_2 = \frac{\tilde{\alpha}_2}{F_\pi^2}\left(\frac{m_\pi^{\rm ph}}{\Lambda_\chi}\right)^2, \tag{16}$$

where the values of $\{\alpha_0, \alpha_2, \tilde{\alpha}_2\}$ from our best fit to the data are $\alpha_0 \approx -0.12$, $\alpha_2 \approx 0.20$ and $\tilde{\alpha}_2 \approx 0.42$, consistent with expectations.

To estimate the impact of the $\mathcal{O}(Q^4)$ terms, we allow α_4 and $\tilde{\alpha}_4$ to vary from -1 to $+1$. This range is considered conservative, given that the values of $\{\alpha_0, \alpha_2, \tilde{\alpha}_2\}$ are smaller. The uncertainty associated with the truncation of the chiral expansion is shown in Fig. 7 (see the green and blue bands). To obtain these bands, we use the best fit parameters for C_0, C_2 and D_2 from our NLO results and supplement the calculations with the higher-order potential $V_{\rm cont}^{(4)}$ from Eq. (14). No refit of the phase shifts at $m_\pi = 280$ MeV was performed, resulting in a more conservative estimate. It is reassuring that the spread in the results at $m_\pi = 280$ MeV is quite natural, and it appears to be comparable in size to the statistical uncertainty from Fig. 5. The resulting uncertainty grows with ξ, but it remains comparable with the statistical error in Fig. 5.

In Fig. 7, we also illustrate the cutoff dependence of the pole trajectory, by comparing the results of the best fits for two cutoffs: $\Lambda = 700$ MeV and $\Lambda = 500$ MeV. As expected, this dependence appears very mild after the refit, and falls well within the truncation error.

Additionally, we verified that the change in $\mathrm{Im}\,E_{\rm pole}$ of the T_{cc} at the physical pion mass, due to the inclusion of the contact term C_2, with this LEC fixed at $m_\pi = 280$ MeV, is very small after adjusting C_0 to reproduce $\mathrm{Re}\,E_{\rm pole}$, and remains well within the uncertainty estimated in Ref. [17].

Finally, another potential source of uncertainty arises from the transition between the real world and the isospin limit at the physical pion mass. As discussed above, the parameter C_0 was adjusted to reproduce the real part of the T_{cc} pole position, $\mathrm{Re}\,E_{\rm pole} = -356$ keV, as extracted from the coupled-channel analysis in Ref. [17]. However, in the isospin limit, the T_{cc} becomes slightly more bound. To estimate the impact of this effect on the pole trajectory, we adopt the following strategy: (i) Starting from the contact coupled-channel framework of Ref. [17] (see fit 1 in Tables I and II), we use the extracted value of C_0 to calculate the T_{cc} pole in the isospin limit, which gives $\mathrm{Re}\,E_{\rm pole} \approx -940$ keV; (ii) Relying on the fact that $\mathrm{Re}\,E_{\rm pole}$ at the physical pion mass is largely insensitive to pion dynamics [17], we use this binding energy as input in the full pionful framework in the isospin limit, recalculate C_0,[2] and find that the impact of this effect on the pole trajectory is very minor (just slightly larger than the effect of cutoff variation shown in Fig. 7). As expected for a more attractive potential, all transitions (quasi-bound to bound, to virtual, to resonance) occur at slightly larger pion masses.

4.2. Comparison to other works

Here, we briefly comment on other lattice calculations available in the literature and compare them with our results. In Ref. [28], the HAL QCD method was utilized to extract the DD^* scattering potential at the pion mass $m_\pi = 146.4$ MeV, which was then employed to calculate the phase shifts above the DD^* threshold. No visible signature of the OPE was observed. Employing the ERE, the T_{cc} pole was reported to be a virtual state with $k = (-8 \pm 8^{+3}_{-5})i$ MeV corresponding to $E_{\rm pole} = -59^{\,+53\,+2}_{\,-99\,-67}$ keV, where the errors represent statistical and systematic uncertainties, in order. Extrapolation of the HAL QCD potential to the physical pion mass, neglecting three-body and isospin violating effects, led to a bound state but with a binding energy substantially smaller than observed experimentally.

The pion mass $m_\pi = 146.4$ MeV corresponds to $\xi \approx 1.07$, with the $DD\pi$ threshold above the DD^* threshold. Thus the three-body decay is already closed but the system experiences the left-hand cut from the OPE. The pole in our approach corresponds to a bound state with $k = (19 \pm 1)i$ MeV and $E_{\rm pole} = -179 \pm 25$ keV. While our pole position is different to that of HAL QCD quantitatively, one may still conclude that the results are qualitatively consistent, as a small modification in the potential is typically sufficient to shift the pole from a bound to a virtual state.

To summarize this discussion, the OPE has a significant effect on the imaginary part of the pole location of the T_{cc} for the physical pion mass. This width is primarily due to the hadronic decay of the T_{cc} to $DD\pi$, with the strength of the OPE controlled by the observable $D^* \to D\pi$ decay. A small increase in the pion mass by about 7% does not change the pion coupling significantly, so that the strength of the OPE

[2] Note that we cannot directly use C_0 from the coupled-channel *pionful* fit of [17] in the isospin limit for the following reasons: (i) unlike Du et al., we employ a formalism with relativistic pions; (ii) in the full approach with pions, C_0 is known to exhibit a limit cycle, meaning it can rapidly change from $-\infty$ to $+\infty$ as a function of the cutoff [67,68] while the observables remain cutoff independent. Due to these reasons, taking C_0 from one pionful framework and applying it in a different one could lead to large, uncontrolled systematic errors. This, however, is expected to work well in the contact case.

at $m_\pi = 146.4$ MeV remains comparable to that at the physical point. On the other hand, the effect of the OPE on the real part of the pole is not so dramatic for pion masses close to the physical point. Indeed, it follows from Fig. 6 that for pion masses $m_\pi \lesssim 230$ MeV ($\xi \lesssim 1.7$), very precise lattice simulations would be required to quantitatively discriminate between the pure contact and pionful results. However, the impact of the OPE for $m_\pi \gtrsim 230$ MeV is very significant since the repulsion generated by the OPE shifts the pole into the complex plane, creating substantial differences from contact results.

In Ref. [27], the charm-quark mass dependence of the T_{cc} pole position was investigated for a pion mass $m_\pi = 280$ MeV and several values of the heavy-quark mass. While the phase shifts were extracted from the FV spectra using the Lüscher method, ignoring the left-hand cuts, the T_{cc} pole position was calculated from fits to the phase shifts in a framework involving the OPE. The pion mass dependence of the T_{cc} pole position was also briefly discussed but very qualitatively, without making quantitative predictions for the pole trajectory.

In Ref. [25], elastic DD^* scattering in S-wave was investigated at $m_\pi \approx 348.5$ MeV. However, the study was limited by using only a single lattice volume and having only one data point in the near-threshold region. As a result of the ERE fits to the phase shifts obtained using the Lüscher method, the effective range parameters were presented – the scattering length and the effective range. Using these parameters, we extracted the pole which turns out to be a virtual state with the energy about -28^{+4}_{-5} MeV, as shown in Fig. 6 by the green dot. While this result ignores the physics related with long-range interactions, it appears consistent with our prediction based on contact EFT.

Very recently, a lattice investigation of coupled $DD^* - D^*D^*$ scattering at $m_\pi = 391$ MeV was presented in Ref. [26], finding a sizable coupled-channel effect. Using the Lüscher method and parameterizations of the coupled-channel amplitudes that ignore the OPE, two states were found in the energy plane: a virtual state about 62(34) MeV below the DD^* threshold and a resonance about $(49(35) + i11(13)/2)$ MeV below the D^*D^* threshold. By employing a contact theory, we can indeed obtain a virtual state around 75 MeV below the DD^* threshold. However, this state transforms into a resonance with a substantially different pole position when the lhc effect from the OPE is included. Further investigations are needed to investigate the impact of the lhc on the coupled-channel transitions and the pole below the D^*D^* threshold.

5. Summary and conclusions

A chiral EFT approach is utilized to establish a continuous connection between the T_{cc} pole position at unphysical pion masses from lattice simulations and the physical world. The effective potential, extended up to next-to-leading order ($\mathcal{O}(Q^2)$), includes three contact terms and the longest range one-pion exchange potential that incorporates all relevant scales associated with the three-body $DD\pi$ cut and the left-hand cut. A proper treatment of these scales is necessary to fulfill analyticity and unitarity of the DD^* scattering amplitude when the pion mass deviates from its physical value. The contact terms are adjusted to reproduce the T_{cc} pole position at the physical pion mass and lattice finite volume spectra at $m_\pi = 280$ MeV. This allows us to predict the trajectory of the T_{cc} pole as a function of the pion mass up to $m_\pi \sim 3m_\pi^{\rm ph}$. To propagate the statistical uncertainty from the lattice data at $m_\pi = 280$ MeV to the pole position at different pion masses, the bootstrap method is employed. Additionally, the truncation uncertainty of chiral EFT is estimated by including two higher-order ($\mathcal{O}(Q^4)$) contact terms based on naturalness.

The resulting position of the pole transitions from a quasi-bound to a bound, a virtual and a resonance state as the pion mass increases, indicating the molecular nature of the T_{cc}. Observing the effect of the OPE on the pole for pion masses slightly above the physical value is challenging and may require very precise lattice simulations. However, for $m_\pi \gtrsim 230$ MeV, the presence of the OPE is evident as the repulsion it generates shifts the pole into the complex plane, leading to substantially different results from those obtained without pions.

Declaration of competing interest

The authors declare that they have no known competing financial interests or personal relationships that could have appeared to influence the work reported in this paper.

Acknowledgements

This work was supported in part by the MKW NRW under the funding code NW21-024-A, by DFG and NSFC through funds provided to the Sino-German CRC 110 “Symmetries and the Emergence of Structure in QCD” (NSFC Grant No. 11621131001, DFG Project-ID 196253076 - TRR 110), by ERC NuclearTheory (grant No. 885150), by BMBF (Contract No. 05P21PCFP1), and by the EU Horizon 2020 research and innovation programme (STRONG-2020, grant agreement No. 824093).

Data availability

Data will be made available on request.

References

[1] A. Esposito, A. Pilloni, A.D. Polosa, Multiquark resonances, Phys. Rep. 668 (2017) 1–97, https://doi.org/10.1016/j.physrep.2016.11.002, arXiv:1611.07920.

[2] R.F. Lebed, R.E. Mitchell, E.S. Swanson, Heavy-quark QCD exotica, Prog. Part. Nucl. Phys. 93 (2017) 143–194, https://doi.org/10.1016/j.ppnp.2016.11.003, arXiv:1610.04528.

[3] F.-K. Guo, C. Hanhart, U.-G. Meißner, Q. Wang, Q. Zhao, B.-S. Zou, Hadronic molecules, Rev. Mod. Phys. 90 (1) (2018) 015004, https://doi.org/10.1103/RevModPhys.90.015004, arXiv:1705.00141.

[4] Y. Yamaguchi, A. Hosaka, S. Takeuchi, M. Takizawa, Heavy hadronic molecules with pion exchange and quark core couplings: a guide for practitioners, J. Phys. G 47 (5) (2020) 053001, https://doi.org/10.1088/1361-6471/ab72b0, arXiv:1908.08790.

[5] N. Brambilla, S. Eidelman, C. Hanhart, A. Nefediev, C.-P. Shen, C.E. Thomas, A. Vairo, C.-Z. Yuan, The XYZ states: experimental and theoretical status and perspectives, Phys. Rep. 873 (2020) 1–154, https://doi.org/10.1016/j.physrep.2020.05.001, arXiv:1907.07583.

[6] F.-K. Guo, X.-H. Liu, S. Sakai, Threshold cusps and triangle singularities in hadronic reactions, Prog. Part. Nucl. Phys. 112 (2020) 103757, https://doi.org/10.1016/j.ppnp.2020.103757, arXiv:1912.07030.

[7] H.-X. Chen, W. Chen, X. Liu, Y.-R. Liu, S.-L. Zhu, An updated review of the new hadron states, Rep. Prog. Phys. 86 (2) (2023) 026201, https://doi.org/10.1088/1361-6633/aca3b6, arXiv:2204.02649.

[8] L. Meng, B. Wang, G.-J. Wang, S.-L. Zhu, Chiral perturbation theory for heavy hadrons and chiral effective field theory for heavy hadronic molecules, Phys. Rep. 1019 (2023) 1–149, https://doi.org/10.1016/j.physrep.2023.04.003, arXiv:2204.08716.

[9] R. Aaij, et al., Observation of an exotic narrow doubly charmed tetraquark, Nat. Phys. 18 (7) (2022) 751–754, https://doi.org/10.1038/s41567-022-01614-y, arXiv:2109.01038.

[10] R. Aaij, et al., Study of the doubly charmed tetraquark T_{cc}^+, Nat. Commun. 13 (1) (2022) 3351, https://doi.org/10.1038/s41467-022-30206-w, arXiv:2109.01056.

[11] A. Feijoo, W.H. Liang, E. Oset, D0D0π+ mass distribution in the production of the Tcc exotic state, Phys. Rev. D 104 (11) (2021) 114015, https://doi.org/10.1103/PhysRevD.104.114015, arXiv:2108.02730.

[12] M.-J. Yan, M.P. Valderrama, Subleading contributions to the decay width of the Tcc+ tetraquark, Phys. Rev. D 105 (1) (2022) 014007, https://doi.org/10.1103/PhysRevD.105.014007, arXiv:2108.04785.

[13] S. Fleming, R. Hodges, T. Mehen, T_{cc}^+ decays: differential spectra and two-body final states, Phys. Rev. D 104 (11) (2021) 116010, https://doi.org/10.1103/PhysRevD.104.116010, arXiv:2109.02188.

[14] S. Navas, et al., Review of particle physics, Phys. Rev. D 110 (3) (2024) 030001, https://doi.org/10.1103/PhysRevD.110.030001.

[15] M. Albaladejo, Tcc+ coupled channel analysis and predictions, Phys. Lett. B 829 (2022) 137052, https://doi.org/10.1016/j.physletb.2022.137052, arXiv:2110.02944.

[16] L. Meng, G.-J. Wang, B. Wang, S.-L. Zhu, Probing the long-range structure of the Tcc+ with the strong and electromagnetic decays, Phys. Rev. D 104 (5) (2021) 051502, https://doi.org/10.1103/PhysRevD.104.L051502, arXiv:2107.14784.

[17] M.-L. Du, V. Baru, X.-K. Dong, A. Filin, F.-K. Guo, C. Hanhart, A. Nefediev, J. Nieves, Q. Wang, Coupled-channel approach to T_{cc}^+ including three-body effects, Phys. Rev. D 105 (1) (2022) 014024, https://doi.org/10.1103/PhysRevD.105.014024, arXiv:2110.13765.

[18] E. Braaten, L.-P. He, K. Ingles, J. Jiang, Triangle singularity in the production of Tcc+(3875) and a soft pion, Phys. Rev. D 106 (3) (2022) 034033, https://doi.org/10.1103/PhysRevD.106.034033, arXiv:2202.03900.

[19] B. Wang, L. Meng, Revisiting the DD* chiral interactions with the local momentum-space regularization up to the third order and the nature of Tcc+, Phys. Rev. D 107 (9) (2023) 094002, https://doi.org/10.1103/PhysRevD.107.094002, arXiv:2212.08447.

[20] L. Dai, S. Fleming, R. Hodges, T. Mehen, Strong decays of Tcc+ at NLO in an effective field theory, Phys. Rev. D 107 (7) (2023) 076001, https://doi.org/10.1103/PhysRevD.107.076001, arXiv:2301.11950.

[21] V. Baru, C. Hanhart, A.E. Kudryavtsev, U.-G. Meißner, The role of the nucleon recoil in low-energy meson nucleus reactions, Phys. Lett. B 589 (2004) 118–124, https://doi.org/10.1016/j.physletb.2004.03.062, arXiv:nucl-th/0402027.

[22] V. Lensky, V. Baru, J. Haidenbauer, C. Hanhart, A.E. Kudryavtsev, U.-G. Meißner, Precision calculation of gamma d —> pi+ nn within chiral perturbation theory, Eur. Phys. J. A 26 (2005) 107–123, https://doi.org/10.1140/epja/i2005-10154-7, arXiv:nucl-th/0505039.

[23] V. Baru, E. Epelbaum, A. Rusetsky, The role of nucleon recoil in low-energy antikaon-deuteron scattering, Eur. Phys. J. A 42 (2009) 111–120, https://doi.org/10.1140/epja/i2009-10845-y, arXiv:0905.4249.

[24] M. Padmanath, S. Prelovsek, Signature of a doubly charm tetraquark pole in DD^* scattering on the lattice, Phys. Rev. Lett. 129 (3) (2022) 032002, https://doi.org/10.1103/PhysRevLett.129.032002, arXiv:2202.10110.

[25] S. Chen, C. Shi, Y. Chen, M. Gong, Z. Liu, W. Sun, R. Zhang, $T_{cc}^+(3875)$ relevant DD^* scattering from $N_f = 2$ lattice QCD, Phys. Lett. B 833 (2022) 137391, https://doi.org/10.1016/j.physletb.2022.137391, arXiv:2206.06185.

[26] T. Whyte, D.J. Wilson, C.E. Thomas, Near-threshold states in coupled $DD^* - D^*D^*$ scattering from lattice QCD, arXiv:2405.15741.

[27] S. Collins, A. Nefediev, M. Padmanath, S. Prelovsek, Toward the quark mass dependence of Tcc+ from lattice QCD, Phys. Rev. D 109 (9) (2024) 094509, https://doi.org/10.1103/PhysRevD.109.094509, arXiv:2402.14715.

[28] Y. Lyu, S. Aoki, T. Doi, T. Hatsuda, Y. Ikeda, J. Meng, Doubly charmed tetraquark Tcc+ from lattice QCD near physical point, Phys. Rev. Lett. 131 (16) (2023) 161901, https://doi.org/10.1103/PhysRevLett.131.161901, arXiv:2302.04505.

[29] M.-L. Du, A. Filin, V. Baru, X.-K. Dong, E. Epelbaum, F.-K. Guo, C. Hanhart, A. Nefediev, J. Nieves, Q. Wang, Role of left-hand cut contributions on pole extractions from lattice data: case study for Tcc(3875)+, Phys. Rev. Lett. 131 (13) (2023) 131903, https://doi.org/10.1103/PhysRevLett.131.131903, arXiv:2303.09441.

[30] M. Lüscher, Volume dependence of the energy spectrum in massive quantum field theories. 2. Scattering states, Commun. Math. Phys. 105 (1986) 153–188, https://doi.org/10.1007/BF01211097.

[31] M. Lüscher, Two particle states on a torus and their relation to the scattering matrix, Nucl. Phys. B 354 (1991) 531–578, https://doi.org/10.1016/0550-3213(91)90366-6.

[32] C.H. Kim, C.T. Sachrajda, S.R. Sharpe, Finite-volume effects for two-hadron states in moving frames, Nucl. Phys. B 727 (2005) 218–243, https://doi.org/10.1016/j.nuclphysb.2005.08.029, arXiv:hep-lat/0507006.

[33] R.A. Briceno, Two-particle multichannel systems in a finite volume with arbitrary spin, Phys. Rev. D 89 (7) (2014) 074507, https://doi.org/10.1103/PhysRevD.89.074507, arXiv:1401.3312.

[34] M. Gockeler, R. Horsley, M. Lage, U.-G. Meißner, P.E.L. Rakow, A. Rusetsky, G. Schierholz, J.M. Zanotti, Scattering phases for meson and baryon resonances on general moving-frame lattices, Phys. Rev. D 86 (2012) 094513, https://doi.org/10.1103/PhysRevD.86.094513, arXiv:1206.4141.

[35] L. Leskovec, S. Prelovsek, Scattering phase shifts for two particles of different mass and non-zero total momentum in lattice QCD, Phys. Rev. D 85 (2012) 114507, https://doi.org/10.1103/PhysRevD.85.114507, arXiv:1202.2145.

[36] S. Aoki, T. Doi, Lattice QCD and baryon-baryon interactions: HAL QCD method, Front. Phys. 8 (2020) 307, https://doi.org/10.3389/fphy.2020.00307, arXiv:2003.10730.

[37] M. Mai, M. Döring, A. Rusetsky, Multi-particle systems on the lattice and chiral extrapolations: a brief review, Eur. Phys. J. Spec. Top. 230 (6) (2021) 1623–1643, https://doi.org/10.1140/epjs/s11734-021-00146-5, arXiv:2103.00577.

[38] P. Bicudo, Tetraquarks and pentaquarks in lattice QCD with light and heavy quarks, Phys. Rep. 1039 (2023) 1–49, https://doi.org/10.1016/j.physrep.2023.10.001, arXiv:2212.07793.

[39] J. Bulava, et al., Hadron spectroscopy with lattice QCD, in: Snowmass 2021, 2022, arXiv:2203.03230.

[40] S. Prelovsek, Spectroscopy of hadrons with heavy quarks from lattice QCD, Nuovo Cimento C 47 (4) (2024) 147, https://doi.org/10.1393/ncc/i2024-24147-3, arXiv:2310.07341.

[41] A.B. Raposo, M.T. Hansen, Finite-volume scattering on the left-hand cut, J. High Energy Phys. 08 (2024) 075, https://doi.org/10.1007/JHEP08(2024)075, arXiv:2311.18793.

[42] S.M. Dawid, M.H.E. Islam, R.A. Briceño, Analytic continuation of the relativistic three-particle scattering amplitudes, Phys. Rev. D 108 (3) (2023) 034016, https://doi.org/10.1103/PhysRevD.108.034016, arXiv:2303.04394.

[43] J.R. Green, A.D. Hanlon, P.M. Junnarkar, H. Wittig, Weakly bound H dibaryon from SU(3)-flavor-symmetric QCD, Phys. Rev. Lett. 127 (24) (2021) 242003, https://doi.org/10.1103/PhysRevLett.127.242003, arXiv:2103.01054.

[44] L. Meng, V. Baru, E. Epelbaum, A.A. Filin, A.M. Gasparyan, Solving the left-hand cut problem in lattice QCD: Tcc(3875)+ from finite volume energy levels, Phys. Rev. D 109 (7) (2024) L071506, https://doi.org/10.1103/PhysRevD.109.L071506, arXiv:2312.01930.

[45] R. Bubna, H.-W. Hammer, F. Müller, J.-Y. Pang, A. Rusetsky, J.-J. Wu, Lüscher equation with long-range forces, J. High Energy Phys. 05 (2024) 168, https://doi.org/10.1007/JHEP05(2024)168, arXiv:2402.12985.

[46] M.T. Hansen, F. Romero-López, S.R. Sharpe, Incorporating DDπ effects and left-hand cuts in lattice QCD studies of the $T_{cc}(3875)^+$, J. High Energy Phys. 06 (2024) 051, https://doi.org/10.1007/JHEP06(2024)051, arXiv:2401.06609.

[47] I. Matuschek, V. Baru, F.-K. Guo, C. Hanhart, On the nature of near-threshold bound and virtual states, Eur. Phys. J. A 57 (3) (2021) 101, https://doi.org/10.1140/epja/s10050-021-00413-y, arXiv:2007.05329.

[48] S. Weinberg, Evidence that the deuteron is not an elementary particle, Phys. Rev. 137 (1965) B672–B678, https://doi.org/10.1103/PhysRev.137.B672.

[49] V. Baru, C. Hanhart, Y.S. Kalashnikova, A.E. Kudryavtsev, A.V. Nefediev, Interplay of quark and meson degrees of freedom in a near-threshold resonance, Eur. Phys. J. A 44 (2010) 93–103, https://doi.org/10.1140/epja/i2010-10929-7, arXiv:1001.0369.

[50] X.-W. Kang, J.A. Oller, Different pole structures in line shapes of the $X(3872)$, Eur. Phys. J. C 77 (6) (2017) 399, https://doi.org/10.1140/epjc/s10052-017-4961-z, arXiv:1612.08420.

[51] P. Junnarkar, N. Mathur, M. Padmanath, Study of doubly heavy tetraquarks in lattice QCD, Phys. Rev. D 99 (3) (2019) 034507, https://doi.org/10.1103/PhysRevD.99.034507, arXiv:1810.12285.

[52] V. Baru, E. Epelbaum, A.A. Filin, C. Hanhart, U.-G. Meißner, A.V. Nefediev, Quark mass dependence of the $X(3872)$ binding energy, Phys. Lett. B 726 (2013) 537–543, https://doi.org/10.1016/j.physletb.2013.08.073, arXiv:1306.4108.

[53] V. Baru, E. Epelbaum, A.A. Filin, J. Gegelia, A.V. Nefediev, Binding energy of the $X(3872)$ at unphysical pion masses, Phys. Rev. D 92 (11) (2015) 114016, https://doi.org/10.1103/PhysRevD.92.114016, arXiv:1509.01789.

[54] H.W. Hammer, S. König, U. van Kolck, Nuclear effective field theory: status and perspectives, Rev. Mod. Phys. 92 (2) (2020) 025004, https://doi.org/10.1103/RevModPhys.92.025004, arXiv:1906.12122.

[55] E. Epelbaum, H. Krebs, P. Reinert, High-precision nuclear forces from chiral EFT: state-of-the-art, challenges and outlook, Front. Phys. 8 (2020) 98, https://doi.org/10.3389/fphy.2020.00098, arXiv:1911.11875.

[56] V. Baru, E. Epelbaum, A.A. Filin, F.-K. Guo, H.-W. Hammer, C. Hanhart, U.-G. Meißner, A.V. Nefediev, Remarks on study of X(3872) from effective field theory with pion-exchange interaction, Phys. Rev. D 91 (3) (2015) 034002, https://doi.org/10.1103/PhysRevD.91.034002, arXiv:1501.02924.

[57] V. Baru, E. Epelbaum, A.A. Filin, C. Hanhart, U.-G. Meißner, A.V. Nefediev, Heavy-quark spin symmetry partners of the X (3872) revisited, Phys. Lett. B 763 (2016) 20–28, https://doi.org/10.1016/j.physletb.2016.10.008, arXiv:1605.09649.

[58] V. Baru, E. Epelbaum, A.A. Filin, C. Hanhart, A.V. Nefediev, Q. Wang, Spin partners W_{bJ} from the line shapes of the $Z_b(10610)$ and $Z_b(10650)$, Phys. Rev. D 99 (9) (2019) 094013, https://doi.org/10.1103/PhysRevD.99.094013, arXiv:1901.10319.

[59] M. Cleven, F.-K. Guo, C. Hanhart, U.-G. Meißner, Light meson mass dependence of the positive parity heavy-strange mesons, Eur. Phys. J. A 47 (2011) 19, https://doi.org/10.1140/epja/i2011-11019-2, arXiv:1009.3804.

[60] D. Becirevic, F. Sanfilippo, Theoretical estimate of the $D^* \to D\pi$ decay rate, Phys. Lett. B 721 (2013) 94–100, https://doi.org/10.1016/j.physletb.2013.03.004, arXiv:1210.5410.

[61] C. Hanhart, J.R. Peláez, G. Ríos, Quark mass dependence of the rho and sigma from dispersion relations and Chiral Perturbation Theory, Phys. Rev. Lett. 100 (2008) 152001, https://doi.org/10.1103/PhysRevLett.100.152001, arXiv:0801.2871.

[62] C. Hanhart, J.R. Peláez, G. Ríos, Remarks on pole trajectories for resonances, Phys. Lett. B 739 (2014) 375–382, https://doi.org/10.1016/j.physletb.2014.11.011, arXiv:1407.7452.

[63] M. Albaladejo, J.A. Oller, On the size of the sigma meson and its nature, Phys. Rev. D 86 (2012) 034003, https://doi.org/10.1103/PhysRevD.86.034003, arXiv:1205.6606.

[64] J.R. Pelaez, G. Rios, Chiral extrapolation of light resonances from one and two-loop unitarized Chiral Perturbation Theory versus lattice results, Phys. Rev. D 82 (2010) 114002, https://doi.org/10.1103/PhysRevD.82.114002, arXiv:1010.6008.

[65] B. Efron, R. Tibshirani, An introduction to the bootstrap, Stat. Sci. 57 (1) (1986) 54–75.

[66] E. Epelbaum, U.-G. Meißner, W. Gloeckle, Nuclear forces in the chiral limit, Nucl. Phys. A 714 (2003) 535–574, https://doi.org/10.1016/S0375-9474(02)01393-3, arXiv:nucl-th/0207089.

[67] A. Nogga, R.G.E. Timmermans, U. van Kolck, Renormalization of one-pion exchange and power counting, Phys. Rev. C 72 (2005) 054006, https://doi.org/10.1103/PhysRevC.72.054006, arXiv:nucl-th/0506005.

[68] V. Baru, A.A. Filin, C. Hanhart, Y.S. Kalashnikova, A.E. Kudryavtsev, A.V. Nefediev, Three-body $D\bar{D}\pi$ dynamics for the $X(3872)$, Phys. Rev. D 84 (2011) 074029, https://doi.org/10.1103/PhysRevD.84.074029, arXiv:1108.5644.